NANO · MICRO small
www.small-journal.com

Spark Discharge Doping—Achieving Unprecedented Control over Aggregate Fraction and Backbone Ordering in Poly(3-hexylthiophene) Solutions

*Fabian Eller, Felix A. Wenzel, Richard Hildner, Remco W. A. Havenith, and Eva M. Herzig**

The properties of semiconducting polymers are strongly influenced by their aggregation behavior, that is, their aggregate fraction and backbone planarity. However, tuning these properties, particularly the backbone planarity, is challenging. This work introduces a novel solution treatment to precisely control the aggregation of semiconducting polymers, namely current-induced doping (CID). It utilizes spark discharges between two electrodes immersed in a polymer solution to create strong electrical currents resulting in temporary doping of the polymer. Rapid doping-induced aggregation occurs upon every treatment step for the semiconducting model-polymer poly(3-hexylthiophene). Therefore, the aggregate fraction in solution can be precisely tuned up to a maximum value determined by the solubility of the doped state. A qualitative model for the dependences of the achievable aggregate fraction on the CID treatment strength and various solution parameters is presented. Moreover, the CID treatment can yield an extraordinarily high quality of backbone order and planarization, expressed in UV–vis absorption spectroscopy and differential scanning calorimetry measurements. Depending on the selected parameters, an arbitrarily lower backbone order can be chosen using the CID treatment, allowing for maximum control of aggregation. This method may become an elegant pathway to finely tune aggregation and solid-state morphology for thin-films of semiconducting polymers.

1. Introduction

A major branch of organic semiconductor research deals with understanding and optimizing morphology. In this field, particularly intensive work is done on polymer aggregation as it paves the way toward efficient charge transport.[1–4] Moreover, the altered aggregate absorption spectrum enables harvesting a broader spectral range of light. The most common ways of influencing aggregation are thermal annealing, solvent vapor annealing, processing from a mixture of good solvents with fractions of marginal or poor solvents, and using other solvent additives.[5–8] Some of these methods are post-treatment steps for the dried film, while others modify the aggregation behavior during the drying process. Complexity further increases moving from single materials to multi-component blends. Therefore, it is desirable to obtain a well-defined aggregation state already in solution before blending of materials and further processing.

Poor solvent additives have successfully been used to induce pre-aggregation. However, this pre-aggregation has limited control, because such additives can have further effects, like gel formation, and the quality of backbone order is often reduced due to the lower solvent quality.[9–12] The reason for the associated lower backbone ordering is linked to the different mechanisms responsible for the ordering in different molecular directions: backbone

F. Eller, E. M. Herzig
Dynamics and Structure Formation – Herzig Group
University of Bayreuth
Universitätsstraße 30, 95447 Bayreuth, Germany
E-mail: eva.herzig@uni-bayreuth.de
F. A. Wenzel
Macromolecular Chemistry and Bavarian Polymer Institute
University of Bayreuth
Universitätsstraße 30, 95447 Bayreuth, Germany
The ORCID identification number(s) for the author(s) of this article can be found under https://doi.org/10.1002/smll.202207537.

DOI: 10.1002/smll.202207537

R. Hildner
Zernike Institute for Advanced Materials
University of Groningen
Nijenborgh 4, Groningen 9747 AG, The Netherlands
R. W. A. Havenith
Stratingh Institute for Chemistry and Zernike Institute for Advanced Materials
University of Groningen
Nijenborgh 4, Groningen 9747 AG, The Netherlands
R. W. A. Havenith
Ghent Quantum Chemistry Group
Department of Chemistry
Ghent University
Krijgslaan 281 (S3), Gent B-9000, Belgium

ordering, side-chain ordering, and π–π stacking.[13] Depending on the driving forces of the aggregation process, different directions of molecular ordering contribute to a different extent, enabling a higher quality of order in one direction at the cost of the quality of order in one or both other directions.[13,14] As transport properties are mostly influenced by backbone ordering, an aggregation mechanism leading to a high quality of backbone order is of interest.

Doping-induced aggregation can lead to pre-aggregation in solution with the desired high quality of backbone order. Molecular doping results in backbone planarization, which then transfers to the high quality of backbone order in the produced aggregates.[15] Usually, doping is achieved by adding dopant molecules to the polymer solution, for example, F4TCNQ (2,3,5,6-tetrafluoro-7,7,8,8-tetracyanoquinodimethane). A charge transfer between the dopant and the polymer occurs, and the dopant counterions subsequently remain in the solution and also in produced thin films, permanently doping the system.[15–19]

In some cases, permanent doping is desired. However, the most suitable dopant amount for aggregation control and permanent doping is not necessarily identical. Thus, decoupling doping-induced aggregation from permanent doping would be highly beneficial.

Here, we present an approach to exploit doping-induced aggregation without permanently doping the material system. Using this novel current-induced doping (CID) treatment allows us to achieve temporary doping of the polymers leading to an accompanying temporary change of solubility. We demonstrate that this electronic solution treatment works in a wide variety of solvents, including green solvents, and does not require any chemical additives. The CID treatment allows for the systematic control of the aggregate fraction as well as the quality of backbone order of the semiconducting polymer poly(3-hexylthiophene) (P3HT) in solution.

2. Temporary Doping for Aggregation Control

In general, for aggregation to occur, the backbone of a polymer needs to straighten before folding or attaching to an existing aggregate.[20] A doping-induced aggregation pathway known from the literature occurs according to the steps shown in **Figure 1**c: The charge induced by the dopant influences the rigidity of the backbone and decreases the solubility in nonpolar organic solvents compared to the neutral polymer.[16,17,19] Hence, after planarization, the chain folds and forms a single-chain aggregate where the charge is delocalized in the conjugated system and stabilized via π–π stacking.[16] This single-chain aggregate can act as a nucleating site for neutral chains stabilizing the charged aggregate further through additional π–π interactions.[16]

In this paper, we actively aim to exploit this mechanism by temporarily charging some of the backbones electronically. To achieve a uniform charge distribution on the backbone in order to examine the general principle of this doping mechanism, we choose a highly investigated conjugated homopolymer, namely the model polymer P3HT. Using simulations, we demonstrate that doping this backbone results in the planarization step necessary for aggregation. Density functional theory (DFT) simulations show that dihedral rotation between two P3HT monomers is suppressed due to a strongly increased energy barrier when positive charge is added to the monomers (Figure 1a). This results in the planarization of a doped backbone section.

2.1. Proposed Process

To gain specific aggregation control, we choose a process that allows us to temporarily dope a fraction of the polymers within a solution. We achieve this with a strong current through the polymer solution. As displayed in Figure 1b,

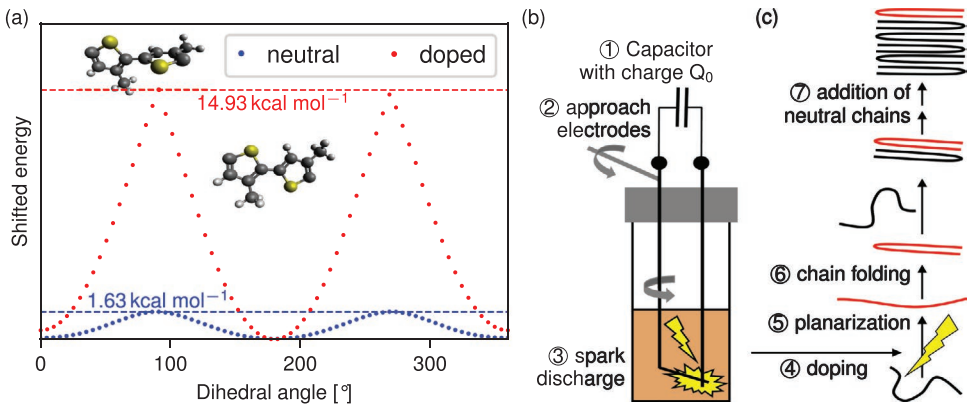

Figure 1. a) Simulation results of energetic profiles (shifted to minimum energy at 180°) upon rotating the dihedral angle between two 3-methylthiophene monomers. The energetic profiles were obtained with DFTB3 simulations and rescaled with the more precise energy barriers obtained from DFT simulations (more details in the Experimental Section and Table S1, Supporting Information). The inserted molecular structures visualize a part of the simulated molecules (consisting of four monomers) at 90° and 180°. b) Schematic diagram of the experimental setup for CID treatment consisting of two tungsten wires connected to a charged capacitor. The field strength between the wires is increased above the breakdown field strength for a spark discharge to occur. This spark results in the doping and, hence, planarization of a polymer chain. c) In doping-induced aggregation, the doped chain (red) can fold and act as a nucleating site for neutral chains (black) to form highly ordered aggregates.[16]

we approach two tungsten wires within our polymer solution connected to a charged capacitor. When the distance between the wires in solution is decreased sufficiently that the electric field strength between the two electrodes is increased above the breakdown field strength, a conductive channel builds up, consisting of ionized solvent and polymer.[21] The strong current flow locally induces evaporation in a small volume around the conductive channel due to Joule heating. This rapid expansion of the evaporating solvent then mixes the solution. Hence, the charged polymer and other ions and radicals generated in the conductive channel are spread across the complete solution. The ion and radical species depend on the solvent, but they are reliably produced, regardless of the solvent. The charged, that is, doped, polymer can start doping-induced aggregation in the complete volume. Moreover, certain ions and radicals can act as dopants and dope further polymer chains increasing the effect. It has to be noted that there may be more than one charge on some of the polymer chains. The doping and resulting aggregation are both demonstrated in the absorption spectra upon CID treatment of P3HT in chloroform (CF). The doped chains give rise to a polaron signature in the low energy region, and the aggregation changes the absorption in the visible region, see Figure S1a, Supporting Information. After the termination of the current and, therefore, also of the energy input, the ionization and radical generation are stopped. The remaining ions and radicals recombine again with counterions and other radicals to neutral non-reactive products. With time the excess charge dissipates in the system and, thus, the doping process and the aggregation stop.

This way, we achieve a fast, temporary, and additive-free doping-induced aggregation of the prototypical semiconducting polymer P3HT.

3. Controlled Increase of Aggregate Fraction

To demonstrate the range of control available with the proposed CID, we systematically investigate the aggregation process and the resulting aggregates as a function of experimental parameters.

Carrying out the CID treatment repeatedly, we can demonstrate a systematic increase in aggregate fraction and analyze the produced aggregates. **Figure 2**a shows solution spectra of 12 mg mL^{-1} P3HT in CF solutions with an increasing number of identical CID treatment steps. Every additional treatment step leads to an increased aggregate absorption, which can be clearly identified by the A_1 and A_2 peaks in the range of 1.9–2.3 eV (related to the 0–0 and 0–1 vibronic transitions of non-aggregated P3HT). To determine the increasing aggregate fraction, we used the approach of scaling an amorphous spectrum to the high-energy shoulder of the obtained absorption spectra at ≥2.6 eV, fitting the A_1–A_5 peaks to the remaining fraction of the spectra and considering the different molar extinction coefficients of the amorphous and aggregated P3HT (details in Experimental Section).[22,23] Figure 2b and further data in Figure 5 demonstrate that in this experiment, the aggregate fraction in solution could be tuned between 0% to at least about 57%, which is a typical value for aggregate fractions in thin films.[24,25] Two references for P3HT without CID treatment are provided, namely, 12 mg mL^{-1} P3HT in CF solutions were 1) left for 25 days at 20 °C (time-induced aggregation) and 2) cooled for 65 min at –18 °C (temperature-induced aggregation), see Figure 2b, blue and green dots. Both procedures yielded aggregate fractions of 2.4% and 5.1%, respectively, which meet the expectations in the good solvent CF.[26]

The aggregate fraction is further influenced by several different parameters. We systematically studied the effect of

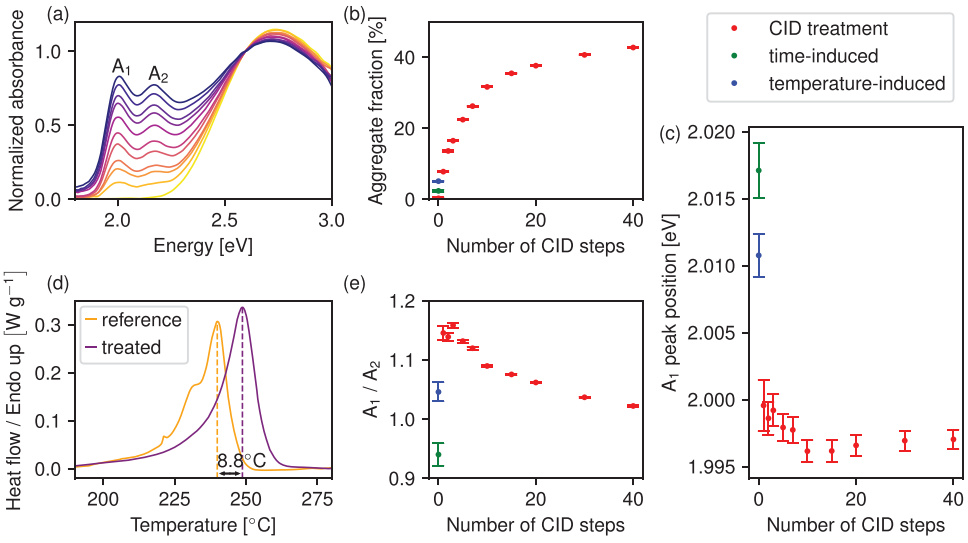

Figure 2. a) Normalized absorption spectra of 12 mg mL^{-1} P3HT in chloroform (CF) solutions with an increasing number of spark treatment steps (from yellow (untreated) to purple (highest number of treatment steps); capacitor charged with 300 V). b,c,e) Results of fitting the vibronic structure (A_1 and A_2 first two peaks; details in Experimental Section) in spectra from (a) and reference spectra of 12 mg mL^{-1} P3HT: 1) left for 25 days at 20 °C (time-induced aggregation) and 2) cooled for 65 min at –18 °C (temperature-induced aggregation). b) Minimum aggregate fraction, c) A_1 peak position, and e) ratio between peak amplitudes of the A_1 to A_2 peak. d) Thermogram of the first DSC heating cycle of 12 mg mL^{-1} P3HT in CF vacuum-dried solutions with CID treatment (purple) and reference without treatment (orange).

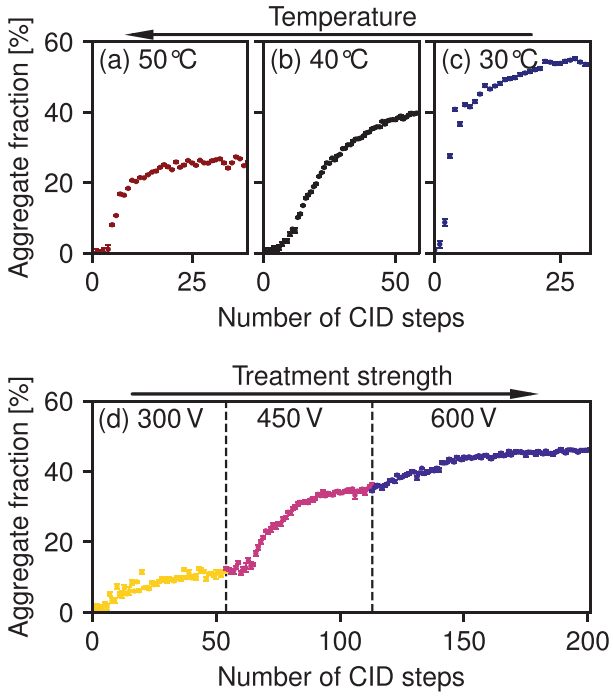

Figure 3. Fit results from associated UV–vis measurements: aggregate fraction in dependency of the number of spark treatment steps for 2 mg mL^{-1} P3HT in tetrahydrofuran (THF) solutions; a–c) with fixed treatment strength (capacitor charged with 600 V), but different temperatures: a) 50 °C, b) 40 °C, and c) 30 °C; d) with the same temperature (40 °C) but consecutively increasing voltage for charging the capacitor from 300 (yellow) to 450 V (pink) and finally 600 V (purple).

temperature, polymer concentration, solvent, poor solvent addition, and CID treatment strength on the achievable aggregate fraction. In **Figure 3**a–c, the aggregate fractions upon CID treatments with 600 V discharges at three different temperatures of 2 mg mL^{-1} P3HT in tetrahydrofuran (THF) solutions are displayed. At all three temperatures, we observe the same general trend. The first CID steps result in a rapid increase in the aggregate fraction. However, the effect due to further CID steps is getting weaker, and a constant value for the aggregate fraction is approached, which we will refer to as the maximum achievable aggregate fraction under a specific set of conditions. This maximum value increases with decreasing temperature. At 30 °C, an aggregate fraction of up to 53% can be achieved, while it is 39% at 40 °C and only 27% at 50 °C. In other words, an aggregate fraction below 27% can be achieved with all three tested temperatures by adjusting the number of treatment steps. However, a lower temperature must be chosen to reach higher aggregate fractions.

Moreover, we increase the treatment strength in a 2 mg mL^{-1} P3HT in THF solution at 40 °C by increasing the voltage for charging the capacitor. With a higher charging voltage, more charge is stored on the capacitor for the spark discharge, and the breakdown field strength is already reached at a larger distance between the two wires. In Figure 3d, the capacitor was at first charged with a voltage of 300 V, resulting in the aggregate fraction leveling off at only 12%. Increasing the voltage to 450 V, the stronger treatment strength increases the achievable aggregate fraction up to 36%. Still on the same solution, the voltage was further increased to 600 V, yielding another increase in the achievable aggregate fraction of up to 46%. Apart from this consecutively increased treatment strength, it is also possible to use one fixed treatment strength (600 V in Figure 3b), resulting in a systematic but not identical increase in aggregate fraction.

We also tested the impact of the polymer concentration and the poor solvent content (see Figure S2, Supporting Information) on the achievable aggregate fractions. The maximum value increases with the polymer concentration and the content of the poor solvent.

4. Quality and Tunability of Backbone Order

While the aggregate fractions can be tuned over a wide range using consecutively increasing as well as a fixed treatment strength, the quality of backbone order is also of great interest in organic electronics. From the absorption spectroscopy data, we can extract information on aggregate properties. The peak positions of the A_1 absorption and the peak ratios between the A_1 and A_2 peaks of the aggregates (obtained from the corresponding fits) reveal information on the quality of backbone order. Compared to the reference samples, the peak positions of the A_1 peak (lower energy peak) show a clear redshift by ≥10 meV (Figure 2c). This shift can be attributed to a higher conjugation length and, thus, to a more planar polymer backbone within the aggregates.[27–29]

The conclusion on the higher backbone ordering for CID aggregates is further supported by the relative changes of the peak ratios between the A_1 and A_2 peaks, where the CID aggregation leads to the highest peak ratios of up to 1.16, Figure 2e. A higher peak ratio results from smaller inter-chain electronic couplings, which result from larger conjugation lengths, and, thus, more planar backbones of the π-stacked polymer chains.[27,30–32]

For subsequent CID steps, the peak ratios between the A_1 and A_2 peaks show a decay with increasing treatment strength. This indicates that the quality of backbone order is slightly decreasing with an increasing number of treatment steps.

The enhanced backbone planarization is further supported by the strong stability of the aggregates revealed by differential scanning calorimetry (DSC) measurements on vacuum-dried polymer solutions. The thermogram of the first heating cycle (Figure 2d) reveals the melting peak of the material with CID treatment at 248.7 °C. This melting peak is with 8.8 °C significantly higher than the melting peak of the untreated reference material at 239.9 °C, which was processed identically except for the CID steps. A peak at 248.7 °C is a surprisingly high value for P3HT. Usually, from the position of the melting peaks, it is possible to calculate ζ, the number of repeating units of the polymer along the chain axis, based on the following relationship[33]

$$\zeta = \frac{a \cdot T_m^0}{T_m - T_m^0} \quad (1)$$

T_m^0 is the melting temperature of a P3HT crystal of infinite size and a is an experimentally derived constant. Snyder et al. obtained

from their study of short P3HT chains without chain folding and oligomers T_m^0 = (545 ± 6) K (272 °C) and a = −5.4 ± 0.5.[33] Using these values and setting the results in relation to literature values of lamellar widths, we can assume an increase in lamellar width of at least 30%.[34,35] This indicates that the planarized parts of the involved backbones need to be significantly longer for the CID-treated P3HT.

Similar results can be achieved by investigating solutions of CID-treated and reference P3HT in CF. Upon heating, the reference P3HT dissolves in CF at around 40 °C, while the P3HT with CID treatment can only be entirely dissolved in CF under sealed conditions at about 80 °C (see Supporting Information).

Re-dissolved P3HT solutions with CID treatment possess a nearly identical molecular weight distribution compared to untreated solutions (Figure S3, Supporting Information). In addition, the second heating curves of the CID-treated sample and the reference feature an almost identical melting peak (Figure S4, Supporting Information). Furthermore, the fact that the CID-treated P3HT can be completely re-dissolved demonstrates the reversibility of the CID treatment. This treatment only forms improved aggregates but does not significantly alter the chemical structure of the polymers permanently.

4.1. Role of Treatment Protocol

Evaluating the absorption spectroscopy data of the experiments with variation in treatment protocol from Figure 3 reveals further information on the formation process. The results in **Figure 4**a show the general tendency that after a range of relatively constant quality of backbone order, that is, constant A_1 peak position, at intermediate aggregate fractions, the quality of backbone order decreases at high aggregate fractions, reflected in the blueshift of the A_1 peak. This decrease is more pronounced and sets in at lower aggregate fractions for the treatment with consecutively increasing strength. At low aggregate fractions, a higher quality of backbone order can be achieved with lower treatment strength (300 V treatment vs 600 V treatment). The values for the A_1 to A_2 peak ratio in Figure 4b, with an initial plateau and a decreasing trend for higher aggregate fractions, support the same conclusion for the impact of the consecutively increasing and fixed treatment strength on the backbone ordering.

Therefore, we can conclude that a lower treatment strength is beneficial at low aggregate fractions, however, limiting the achievable range of aggregate fractions. For high aggregate fractions, a higher fixed treatment strength yields a better aggregate quality than the consecutively increasing treatment strength.

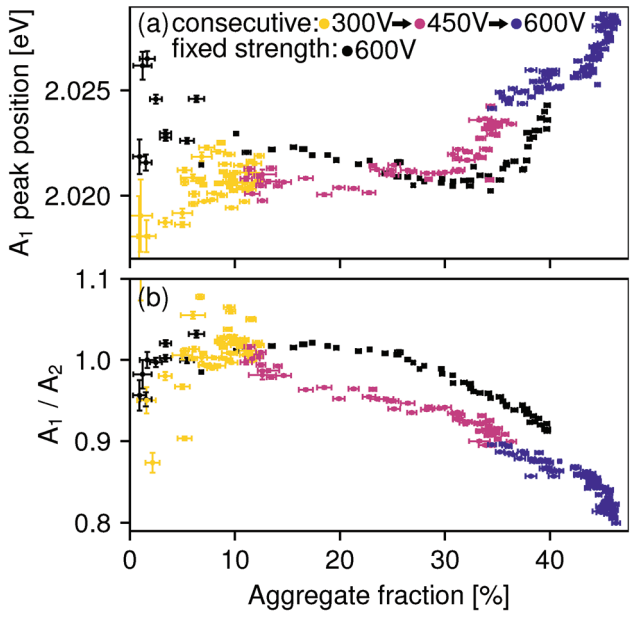

Figure 4. Fit results from associated UV–vis measurements: a) A_1 peak position and b) peak amplitude ratio between A_1 peak and A_2 peak obtained from fitting the vibronic structure from the spectra of the experiments in Figure 3b,d (same color code used).

4.2. Role of Solvent

The CID treatment allows inducing aggregation in various solvents, including green solvents. We examined the CID treatment in the following solvents: chloroform (CF), toluene (TOL), *o*-xylene (OX), tetrahydrofuran (THF), and various mixing ratios of OX and the poor solvent acetonitrile (ACN). For all tested solvents, control over the aggregate fraction can be realized. The main changes between the solvents are systematic differences in the quality of the backbone order. In **Figure 5**a,b, we summarize

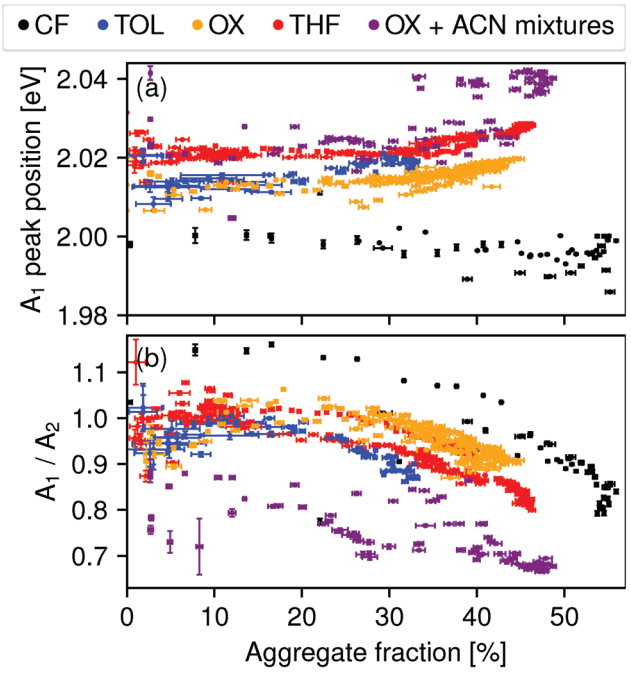

Figure 5. Fit results from associated UV–vis measurements: a) A_1 peak position and b) ratio of the peak amplitudes between the A_1 peak and the A_2 peak obtained from fitting the vibronic structure from more than 600 individual spectra obtained in more than 30 independent CID treatments series. The data are categorized by the used solvents: chloroform (CF, black), toluene (TOL, blue), *o*-xylene (OX, orange), tetrahydrofuran (THF, red), and various mixing ratios of *o*-xylene and acetonitrile (OX + ACN mixtures, purple).

the results of fitting more than 600 spectra obtained in more than 30 independent CID treatment series, mainly using various non-chlorinated solvents. All datasets from one solvent are shown in a single color. The A_1 peak position, as well as the peak ratios of the absorption spectroscopy data, shows the same systematic tendencies: The quality of the backbone order is decreasing at high aggregate fractions after relatively constant values at intermediate and low aggregate fractions. Aggregates in CF possess an exceptionally high quality of backbone order. For the other solvents, the overall quality of backbone order can be correlated with the polarity of the solvents. A high Hansen polarity parameter δ_p indicates a high solvent polarity. While *o*-xylene (δ_p = 1.0 MPa) and toluene (δ_p = 1.4 MPa) have the lowest polarity, they show the highest backbone ordering, THF (δ_p = 5.7 MPa) shows a lower backbone ordering.[36] The ACN (δ_p = 18.0 MPa) admixture to OX further boosts the solvent polarity and results in the lowest quality of backbone order.[36]

5. Discussion

5.1. Aggregate Formation

Examining CID in CF (see Figures 2 and 5), we showed that direct control of the aggregate fraction between 0% and at least about 57% could be achieved with the CID treatment. The extracted information on backbone ordering supports our assumed model for aggregate formation because high-quality aggregates are formed particularly for the initial CID steps, which is shown in a clear redshift of the A_1 peak, a high A_1 to A_2 peak ratio, and the strong shift to higher melting temperatures in DSC (Figure 2c–e). Combined with the apparent polaron absorption (Figure S1, Supporting Information), we conclude that the backbone's planarization occurs due to doping. Those more planar chains are then incorporated into aggregates, explaining the high planarity in the aggregates. Moreover, the increased backbone stiffness upon doping observed in the simulations in Figure 1a supports suppressed chain folding resulting in a more extended lamellar width.

In general, each CID step results in further aggregation events. Initially, mainly the long and defect-free chains aggregate.[10,37–39] Subsequent treatment steps induce aggregates with lower quality, gradually decreasing the observed average quality of backbone order since more and more chain-ends and regiodefects must be incorporated, which causes torsional disorder along P3HT backbones within aggregates.

5.2. Tunability of Aggregate Fraction

The simplest way to control the aggregate fraction is by monitoring the aggregate fraction with UV–vis absorption spectroscopy and stopping the spark treatment when the desired aggregate fraction is achieved. In our measurements, we always observe the same characteristic dependence of the aggregate fraction on the number of treatment steps: the initial substantial increase of aggregate fraction is slowed down until it reaches a plateau at a specific constant aggregate fraction (Figures 2 and 3). Assuming that under fixed processing conditions with a fixed CID treatment strength, a specific fraction of the polymer can be aggregated, this general tendency can be explained purely statistically. A certain portion of the polymer chains gets doped upon a CID treatment step. A fraction of these doped chains starts to aggregate, while another fraction does not aggregate because it cannot form aggregates under the chosen conditions (e.g., defects hampering the aggregation or tie-chains between aggregates). A third fraction of the doped chains does not aggregate because it is already aggregated. With increasing aggregate fraction, the third fraction of the already aggregated chains grows at the cost of the first fraction of chains that can be aggregated. Thus, the aggregation rate decreases with every treatment step until it is 0 because all chains that can be aggregated under the given conditions are already aggregated.

In Figure 3 as well as in Figure S2, Supporting Information, we could demonstrate that by carrying out CID for selected solution parameters (temperature, concentration, and poor solvent additive), we reach a specific achievable aggregate fraction, that is, the level of the plateau reached after sufficient treatment steps. However, the plateau does depend on the treatment strength. To explain the dependencies of the achievable aggregate fraction using CID treatment, we extend the literature models for disorder–order transitions of neutral polymers by a further dimension.

Temperature-induced disorder–order transitions in semiconducting polymers are widely studied.[20,37,40–45] When the temperature of a polymer solution is decreased, the solvent quality decreases, and thus the polymer's solubility decreases accordingly. Upon reducing the temperature, P3HT undergoes a disorder–order transition from a random coil via a planarized coil and a disordered aggregate to a planarized aggregate and possibly a crystallized aggregate.[20] The temperature acts as a parameter controlling the solubility, where for lower solubility, less material is in an amorphous random coil phase and increasingly more material in an aggregated phase.[20,37] Other parameters, such as, for example, poor solvent content and polymer concentration, can have a similar effect, and also other polymers undergo similar disorder–order transitions.[7,10–12,20,40–46] In the following, we will refer to the parameters influencing the solubility, like the polymer concentration, poor solvent concentration, and temperature as solubility parameters.

The clear polaron signature in Figure S1a, Supporting Information, suggests that the strong current flow induced by the CID treatment leads to doping (charging) of the polymer. The solubility of charged polymers is lower compared to the corresponding neutral polymers in the nonpolar organic solvents generally used for semiconducting polymers.[16,17,19] Also, increasing the doping ratio further reduces the polymer's solubility.[18] With a stronger CID treatment, more current is flowing, and we can expect on the one hand a higher number of doped chains and on the other hand higher doping ratios of single chains. Thus, more chains can be aggregated and there is a lower solubility. Therefore, the solubility during CID processing is a) a function of solubility parameters discussed in the previous paragraph and b) a function of the treatment strength. For simplicity, we consider only one solubility parameter in the following, but more could be considered analogously.

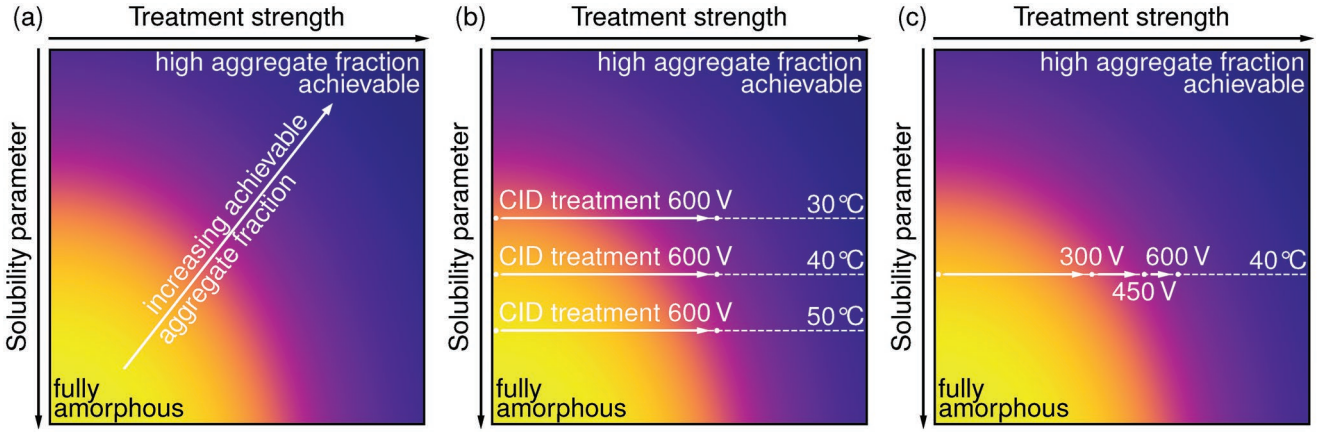

Figure 6. a) Sketch of a qualitative 2D parameter space map displaying the achievable aggregate fraction (plateau reached after sufficient treatment steps) color-coded from yellow (fully amorphous/no aggregation achievable) to purple (high aggregate fraction achievable) as a function of the treatment strength and a solubility parameter. b) Exemplary jumps for spark treatments from Figure 3a–c) with the same treatment strength (capacitor charged with 600 V) at different temperatures (30 °C, 40 °C, and 50 °C) and c) from Figure 3d at the same temperature (40 °C), but consecutively increasing treatment strength (capacitor charged with 300 V, then increased to 450 and 600 V).

Using the solubility parameter as one dimension and the treatment strength as a further dimension, we draw a qualitative 2D parameter space map (scale of solubility and treatment strength qualitative). In this 2D parameter space, the achievable aggregate fraction (plateau reached after sufficient treatment steps) can be displayed as a measure of solubility. The lower the solubility is, the higher the achievable aggregate fraction. In **Figure 6**a, such a 2D map is sketched. The achievable aggregate fraction is color coded from yellow (fully amorphous/no aggregation achievable) to purple (high aggregate fraction achievable). The polymer is nearly fully amorphous with a high solubility parameter and low treatment strength.[47] By decreasing the solubility parameter and/or increasing the treatment strength, an increasing aggregate fraction is achievable.

On this basis, the measurements in Figure 3 can be discussed. Without CID treatment, the accessible parameter space is the ordinate at 0 treatment strength. Conducting the CID treatment temporarily charging the polymer leads to a temporary, horizontal shift in the qualitative 2D map from 0 treatment strength to a specific treatment strength. These jumps in parameter space are sketched in Figure 6b for three different temperatures (=at three different solubility parameters) representing the measurements in Figure 3a–c. With identical treatment strength, there is always the same horizontal jump. In the example here (Figure 6b), the starting point of the transition is vertically shifted due to carrying out the treatment at different solubility parameters (by using different temperatures). Only minimal aggregation occurs at the starting point for all three sketched temperatures (e.g., first absorption spectrum in Figure 2a). However, with the CID treatment, the now charged polymer temporarily experiences an environment with higher aggregation tendency leading to significant aggregate fractions for repeated CID treatments. The largest aggregate fractions from Figure 3a–c are achieved at 30 °C, followed by 40 °C, and the lowest at 50 °C, because the jump occurs into a region with larger (30 °C) or smaller (50 °C) aggregation tendency as seen from the 2D parameter space maps. The aggregates are still stable at the initial condition since only the formation is suppressed at that condition and not the final state.

Analogous 2D maps of the achievable aggregate fraction with the spark treatment can also be drawn in dependence on other solubility parameters as, for example, poor solvent content or polymer concentration, as shown in Figure S5, Supporting Information. It is important to note that there are also conditions where no aggregation occurs upon CID treatment (e.g., in Figure S2c, Supporting Information).

The 2D parameter space maps also explain the aggregation behavior if the solubility parameter is kept constant and the treatment strength is adjusted. Figure 6c shows the induced jumps in parameter space with different CID treatment strengths (data in Figure 3d). The jump for 300 V is still parallel to the treatment strength axis but shorter than in Figure 6b with 600 V. With the consecutive increase of voltage, the overall jump depth is increased, allowing for an increased achievable aggregate fraction.

Thus, the qualitative model presented here can explain a large variety of results of the achievable aggregate fraction and, therefore, can be used as a guide to choose experimental conditions to achieve the desired aggregate fractions for various material systems.

The different results obtained by increasing the CID treatment strength consecutively up to a specific strength compared to a treatment with the same fixed treatment strength are due to the different starting point of the 600 V treatment. From Figure 4 it is clear that the aggregate properties after the 450 V treatment are different to the aggregate properties at the same aggregate fraction with a fixed treatment strength of 600 V. This will be discussed in more detail in the following section. Depending on the properties of the already existing aggregates and the remaining amorphous chains different fractions of the involved material are accessible for aggregation.

5.3. Tunability of Aggregate Properties

Our 2D parameter space maps only allow a statement about the achievable aggregate fraction, while the aggregate properties

(e.g., quality of molecular ordering and aggregate size) must be considered separately and will highly depend on the chosen processing path. With the results from UV–vis spectroscopy, we mainly access the quality of backbone order, which is of great importance for charge transport.

Considering the basics leading to the 2D parameter space map for the achievable aggregate fraction can also explain the differences observed in the backbone ordering. A low treatment strength only achieves aggregation of long and defect-free polymer chains.[10,37–39] Defect-free chains naturally have a higher quality of packing. Therefore, high-quality backbone ordering can be expected for the low voltage (=low treatment strength). When in contrast, a stronger treatment strength is used, it is likely that already in the first treatment steps, shorter and defective chains are among the aggregated material. Therefore, the average order is lower, supporting the results in the low aggregate fraction range in Figure 4. An increasing doping ratio due to a stronger treatment strength leads to a stronger planarization of the polymer chains prior to chain folding. This can translate to an increased backbone ordering in the aggregates, which we observe in Figure 4 at higher aggregate fractions.

Comparing the different solvents in Figure 5, the backbone ordering upon CID treatment appears to be correlated with solvent polarity (for the tested non-chlorinated solvents). Taking selective backbone and sidechain solubility into consideration, our hypothesis is that the polarity of the solvent compared to the sidechains and the charged backbone is decisive.[48] While the hexyl sidechains are nonpolar (note, *n*-hexane, chemically similar to the sidechains, has a vanishing Hansen polarity parameter of $\delta_p = 0$ MPa), the polymer backbones charged by the CID treatment are polar.[36] The polarity of all used solvents can be expected to lie between the polarity of the sidechain and the charged backbone. Considering a very nonpolar solvent, the aggregation would be expected to be driven by the stacking of the charged backbones leading to a strong backbone ordering. With increasing polarity of the solvent, the affinity between the sidechains is increasingly contributing to the driving forces of the aggregation. In this case, sidechain ordering and backbone ordering are both contributing, and the quality of the backbone order suffers in a more polar solvent.[13,14]

Compared with the non-chlorinated solvents, CID treatment in CF leads to exceptionally high backbone ordering despite possessing a higher polarity ($\delta_p = 3.1$ MPa) than *o*-xylene and toluene.[36] One reason causing an increased planarization during the CID treatment could be an exceptionally high and sufficiently long-lived doping ratio achieved in CF. For a more strongly charged backbone, the backbone aggregation dominates the side chain aggregation stronger than if less charged. If the doping is strong enough, this can then compensate for the slightly higher solvent polarity. In contrast to other solvents, we observed a characteristic polaron absorption in CF solutions upon CID treatment (Figure S1, Supporting Information), which supports the hypothesis of a high doping ratio.[49–52] This strong doping is probably possible due to several factors. Due to the intrinsic instability of CF and its function as a Lewis acid, P3HT chains in CF are, on average, slightly positively charged even without spark treatment.[53,54] We already demonstrated this property in a previous work by the positive electrophoretic mobility of P3HT in CF and used it to move P3HT in a wet thin film driven by an electric field.[55] If P3HT is further positively charged beyond this intrinsic effect, that is, further electrons are transferred from P3HT to CF, charge remains localized on the P3HT for a longer time. The reason is that the CF^- anion is unstable, and a Cl^- anion splits off upon charging a CF molecule negatively.[56–58] A $HCl_2C^\bullet$ radical is left behind, and the Cl^- anion forms a quite stable and long-lived cluster anion with a neutral CF molecule stabilizing the doped P3HT.[56,57] With this slower decay of the P3HT doping ratio, a stronger and more ordered aggregation can be achieved in CF compared to the other (non-chlorinated) solvents, explaining the exceptional role of the solvent CF we observe in Figure 5. This longer lifetime is also in line with the possibility to observe the polaron absorption in CF, but not in other solvents (Figure S1, Supporting Information).

6. Conclusion

We developed a novel solution treatment for controlled polymer aggregation. CID utilizes spark discharges between two tungsten electrodes immersed in a polymer solution. This treatment induces a fast subsequent aggregation process, which we monitor for every treatment step by absorption spectroscopy. We show that the aggregation process is a special form of doping-induced aggregation, where strong electric currents through the solution can be used to quickly switch on and off doping.

Our newly presented CID treatment aims to achieve maximum control over the polymer aggregation process in several ways. We demonstrated a stepwise control for setting the aggregate fraction in various solvents. Moreover, we introduced a qualitative model describing the achievable aggregate fraction as a function of solubility parameters (e.g., temperature, polymer concentration, or poor solvent content) and the treatment strength. The tunability of the achievable aggregate fraction proposed by our model is in good agreement with numerous experiments examining various solubility parameters (temperature, polymer concentration, and poor solvent content) and experimental settings (CID treatment strength).

Beyond the control over the aggregate fraction, we can also control the backbone ordering with the CID treatment. This is partially possible by choosing an appropriate treatment strength, but the highest control is possible by choice of solvent. Particularly the solvent polarity appears to be an essential factor where nonpolar solvents can yield the highest backbone order among the tested non-chlorinated solvents. The highest backbone order among all tested solvents could be achieved with CF. The other extreme case of the lowest backbone order could be achieved by admixtures of the highly polar solvent ACN. Therefore, a broad spectrum of backbone ordering can be achieved with the CID treatment by rationally choosing the solvent.

We demonstrated that our approach of exploiting the CID treatment can be successfully employed to control the aggregation state of P3HT in solution before further processing. Therefore, this method may become an elegant pathway to finely tune aggregation and solid-state morphology for thin-films of semiconducting polymers, especially if employed for

multi-component systems, like binary donor–acceptor mixtures. We further anticipate that this CID treatment can also be transferred to other semiconducting polymers to control their aggregation in solution. These solutions can be further processed to dried films and will be investigated next.

7. Experimental Section

Materials: P3HT with a regioregularity of 96% was purchased from Rieke Metals (size exclusion chromatography (SEC) data on molecular weight in Figure S3, Supporting Information), chloroform from Sigma-Aldrich, THF from Fisher Chemical, *o*-xylene from Alfa Aesar and toluene as well as ACN from VWR Chemicals. All materials were used as received.

CID Treatment: The untreated P3HT solutions were prepared by dissolving P3HT in the specified solvent at 50 °C for 20 min. Prior to the CID treatment, the solutions were kept for 15 min at the desired temperature to allow for proper equilibration. This temperature was also kept constant throughout the complete CID treatment. As seen in the schematic diagram of the setup for the CID treatment in Figure 1b, a capacitor (WIMA MKS 4, 3.3 µF) was charged to the specified voltage and subsequently connected to two tungsten wires separated by several millimeters and immersed into the P3HT solution. These two tungsten wires were then approached until a spark discharge occurred below a separation of 1 mm before the wires are brought into contact. This procedure of charging the capacitor, connecting, and approaching the tungsten wires was repeated until the desired number of CID treatment steps was achieved. A photograph of the comparison between an untreated solution and a solution with CID treatment is displayed in Figure S6, Supporting Information. A safety evaluation for each solvent was carried out prior to the start of experiments.

UV–Vis Absorption Spectroscopy: For acquiring the UV–vis absorption measurements, a combined deuterium and halogen white light source from Ocean Optics and an AvaSpec-HSC1024 × 58 TEC-EVO spectrometer from Avantes were used to measure the absorption of the solutions. Short optical path lengths in the range of 100 µm and less were realized by time-resolved measurements of wet thin films with a time resolution of 6 ms. Spectra were evaluated before any drying dynamics occurred. Amorphous spectra measured at the same concentration and temperature in the same solvent were scaled to the high-energy shoulder of the absorption spectrum at ≥2.6 eV.[22,23] This rescaled amorphous spectrum was subsequently subtracted from the absorption spectrum, which was then fitted by the sum of five equidistant (distance of 0.17 eV between peaks) gaussian peaks for the A_1 to A_5 peaks.[22,23] While an identical peak width was fitted for the A_2 to A_5 peaks, a smaller peak width was fitted for the A_1 peak.[59,60] The minimum aggregate fraction was calculated using the area below the fits and below the rescaled amorphous spectrum considering the different molar extinction coefficients of the amorphous and aggregated P3HT described by Clark et al.[23] This procedure yields an estimate for the minimum aggregate fraction as higher optical transitions of the aggregate can contribute to the high energy shoulder leading to an overestimation of the amorphous absorption.

Simulations: The energy barriers upon dihedral rotation of the backbone of poly(3-methylthiophene) oligomers including four monomers without charge and with a charge of +1e were simulated using the Amsterdam Modeling Suite (AMS). In AMS, potential energy scans of the S—C—C—S dihedral angle were used exploiting DFTB3, an extension of the self-consistent-charge density-functional tight-binding method.[61,62] To obtain more precise results, we also conducted DFT simulations for the syn (0°), transition state (90°), and anti (180°) conformation with AMS using B3LYP/TZ2P.[63–67] While the minima at 0° and 180° were fully optimized, for the transition state, a constrained optimization was performed with the S—C—C—S dihedral angle fixed to 90°. The DFTB3 PES scans were rescaled to fit the energy difference between the transition state and the anti-conformation obtained with DFT.

Differential Scanning Calorimetry: DSC was performed using a Mettler Toledo DSC 3+. For the preparation of solid samples, differently treated solutions of P3HT were prepared, and the solvent was removed entirely under vacuum overnight. About 3–10 mg of the dried samples was weighed into DSC pans, which were then closed with a cover lid. All samples were heated from 50 to 300 °C under nitrogen. The cooling and heating rates were always 10 K min^{-1}. The reported melting temperatures refer to peak temperatures in the DSC thermograms. The DSC data were corrected by a baseline correction.

Supporting Information

Supporting Information is available from the Wiley Online Library or from the author.

Acknowledgements

F.E. and E.M.H. thank for funding from SolarEraNet (No. NFA4R2ROPV). F.E. and F.A.W. thank the Elite Study Program Macromolecular Science within the Elite Network of Bavaria (ENB) for support. The authors are grateful to Florian Meichsner (Macromolecular Chemistry, University of Bayreuth) for help with the SEC measurements. The simulation work was performed under the Project HPC-EUROPA3 (INFRAIA-2016-1-730897), with the support of the EC Research Innovation Action under the H2020 Programme; in particular, F.E. gratefully acknowledges the Stratingh Institute for Chemistry and the computer resources and technical support provided by SURF.

Open access funding enabled and organized by Projekt DEAL.

Conflict of Interest

The authors declare no conflict of interest.

Data Availability Statement

The data that support the findings of this study are available from the corresponding author upon reasonable request.

Keywords

conjugated polymers, density functional theory, green solvents, nanostructural control, organic semiconductors, solubility, solution pre-aggregation

Received: December 2, 2022
Revised: January 27, 2023
Published online: March 2, 2023

[1] H. Sirringhaus, P. J. Brown, R. H. Friend, M. M. Nielsen, K. Bechgaard, B. M. W. Langeveld-Voss, A. J. H. Spiering, R. A. J. Janssen, E. W. Meijer, P. Herwig, D. M. De Leeuw, *Nature* **1999**, *401*, 685.
[2] H. Wang, Y. Xu, X. Yu, R. Xing, J. Liu, Y. Han, *Polymers* **2013**, *5*, 1272.
[3] R. Noriega, J. Rivnay, K. Vandewal, F. P. V. Koch, N. Stingelin, P. Smith, M. F. Toney, A. Salleo, *Nat. Mater.* **2013**, *12*, 1038.
[4] Z.-Y. Wang, L. Di Virgilio, Z.-F. Yao, Z.-D. Yu, X.-Y. Wang, Y.-Y. Zhou, Q.-Y. Li, Y. Lu, L. Zou, H. I. Wang, X.-Y. Wang, J.-Y. Wang, J. Pei, *Angew. Chem.* **2021**, *133*, 20646.

[5] S. Pröller, D. Moseguí González, C. Zhu, E. Schaible, C. Wang, P. Müller-Buschbaum, A. Hexemer, E. M. Herzig, *Rev. Sci. Instrum.* **2017**, *88*, 066101.
[6] G. Shi, J. Yuan, X. Huang, Y. Lu, Z. Liu, J. Peng, G. Ding, S. Shi, J. Sun, K. Lu, H.-Q. Wang, W. Ma, *J. Phys. Chem. C* **2015**, *119*, 25298.
[7] L. Li, G. Lu, X. Yang, *J. Mater. Chem.* **2008**, *18*, 1984.
[8] G. L. Schulz, S. Ludwigs, *Adv. Funct. Mater.* **2017**, *27*, 1603083.
[9] C. E. Johnson, M. P. Gordon, D. S. Boucher, *J. Polym. Sci., Part B: Polym. Phys.* **2015**, *53*, 841.
[10] S. Berson, R. De Bettignies, S. Bailly, S. Guillerez, *Adv. Funct. Mater.* **2007**, *17*, 1377.
[11] S. Ludwigs, *P3HT Revisited – From Molecular Scale to Solar Cell Devices*, Springer, Berlin **2014**.
[12] N. Kiriy, E. Jähne, H.-J. Adler, M. Schneider, A. Kiriy, G. Gorodyska, S. Minko, D. Jehnichen, P. Simon, A. A. Fokin, M. Stamm, *Nano Lett.* **2003**, *3*, 707.
[13] Z. Peng, L. Ye, H. Ade, *Mater. Horiz.* **2022**, *9*, 577.
[14] J. H. Carpenter, M. Ghasemi, E. Gann, I. Angunawela, S. J. Stuard, J. J. Rech, E. Ritchie, B. T. O'connor, J. Atkin, W. You, D. M. Delongchamp, H. Ade, *Adv. Funct. Mater.* **2019**, *29*, 1806977.
[15] J. Gao, J. D. Roehling, Y. Li, H. Guo, A. J. Moulé, J. K. Grey, *J. Mater. Chem. C* **2013**, *1*, 5638.
[16] F. M. Mcfarland, C. M. Ellis, S. Guo, *J. Phys. Chem. C* **2017**, *121*, 4740.
[17] L. Müller, D. Nanova, T. Glaser, S. Beck, A. Pucci, A. K. Kast, R. R. Schröder, E. Mankel, P. Pingel, D. Neher, W. Kowalsky, R. Lovrincic, *Chem. Mater.* **2016**, *28*, 4432.
[18] A. E. Mansour, D. Lungwitz, T. Schultz, M. Arvind, A. M. Valencia, C. Cocchi, A. Opitz, D. Neher, N. Koch, *J. Mater. Chem. C* **2020**, *8*, 2870.
[19] M. Arvind, C. E. Tait, M. Guerrini, J. Krumland, A. M. Valencia, C. Cocchi, A. E. Mansour, N. Koch, S. Barlow, S. R. Marder, J. Behrends, D. Neher, *J. Phys. Chem. B* **2020**, *124*, 7694.
[20] F. Panzer, H. Bässler, A. Köhler, *J. Phys. Chem. Lett.* **2017**, *8*, 114.
[21] S. Ray, *An Introduction to High Voltage Engineering*, 2nd ed., PHI Learning, Delhi, **2014**.
[22] C. Scharsich, R. H. Lohwasser, M. Sommer, U. Asawapirom, U. Scherf, M. Thelakkat, D. Neher, A. Köhler, *J. Polym. Sci., Part B: Polym. Phys.* **2012**, *50*, 442.
[23] J. Clark, J.-F. Chang, F. C. Spano, R. H. Friend, C. Silva, *Appl. Phys. Lett.* **2009**, *94*, 163306.
[24] M. Reichenberger, D. Kroh, G. M. M. Matrone, K. Schötz, S. Pröller, O. Filonik, M. E. Thordardottir, E. M. Herzig, H. Bässler, N. Stingelin, A. Köhler, *J. Polym. Sci., Part B: Polym. Phys.* **2018**, *56*, 532.
[25] M. Reichenberger, S. Baderschneider, D. Kroh, S. Grauf, J. Köhler, R. Hildner, A. Köhler, *Macromolecules* **2016**, *49*, 6420.
[26] F. Machui, S. Langner, X. Zhu, S. Abbott, C. J. Brabec, *Sol. Energy Mater. Sol. Cells* **2012**, *100*, 138.
[27] J. Clark, C. Silva, R. H. Friend, F. C. Spano, *Phys. Rev. Lett.* **2007**, *98*, 206406.
[28] C. A. Sandstedt, R. D. Rieke, C. J. Eckhardt, *Chem. Mater.* **1995**, *7*, 1057.
[29] A. Köhler, H. Bässler, *Electronic Processes in Organic Semiconductors: An Introduction*, Wiley-VCH, Weinheim **2015**.
[30] J. Gierschner, Y.-S. Huang, B. Van Averbeke, J. Cornil, R. H. Friend, D. Beljonne, *J. Chem. Phys.* **2009**, *130*, 044105.
[31] F. C. Spano, *J. Chem. Phys.* **2005**, *122*, 234701.
[32] F. C. Spano, C. Silva, *Annu. Rev. Phys. Chem.* **2014**, *65*, 477.
[33] C. R. Snyder, R. C. Nieuwendaal, D. M. Delongchamp, C. K. Luscombe, P. Sista, S. D. Boyd, *Macromolecules* **2014**, *47*, 3942.
[34] M. Brinkmann, P. Rannou, *Adv. Funct. Mater.* **2007**, *17*, 101.
[35] R. Zhang, B. Li, M. C. Iovu, M. Jeffries-El, G. Sauvé, J. Cooper, S. Jia, S. Tristram-Nagle, D. M. Smilgies, D. N. Lambeth, R. D. Mccullough, T. Kowalewski, *J. Am. Chem. Soc.* **2006**, *128*, 3480.
[36] C. M. Hansen, *Hansen Solubility Parameters: A User's Handbook*, 2nd ed., CRC Press, Boca Raton, FL **2007**.
[37] F. Panzer, H. Bässler, R. Lohwasser, M. Thelakkat, A. Köhler, *J. Phys. Chem. Lett.* **2014**, *5*, 2742.
[38] P. Kohn, S. Huettner, H. Komber, V. Senkovskyy, R. Tkachov, A. Kiriy, R. H. Friend, U. Steiner, W. T. S. Huck, J.-U. Sommer, M. Sommer, *J. Am. Chem. Soc.* **2012**, *134*, 4790.
[39] F. Paquin, H. Yamagata, N. J. Hestand, M. Sakowicz, N. Bérubé, M. Côté, L. X. Reynolds, S. A. Haque, N. Stingelin, F. C. Spano, C. Silva, *Phys. Rev. B* **2013**, *88*, 155202.
[40] A. Köhler, S. T. Hoffmann, H. Bässler, *J. Am. Chem. Soc.* **2012**, *134*, 11594.
[41] L. Sun, J. Zhao, W. Huang, X. Chen, W. Zhang, Y. Ding, L. Li, *J. Polym. Sci., Part B: Polym. Phys.* **2019**, *57*, 1105.
[42] T. Unger, F. Panzer, C. Consani, F. Koch, T. Brixner, H. Bässler, A. Köhler, *ACS Macro Lett.* **2015**, *4*, 412.
[43] C. Scharsich, F. S. U. Fischer, K. Wilma, R. Hildner, S. Ludwigs, A. Köhler, *J. Polym. Sci., Part B: Polym. Phys.* **2015**, *53*, 1416.
[44] M. Reichenberger, J. A. Love, A. Rudnick, S. Bagnich, F. Panzer, A. Stradomska, G. C. Bazan, T.-Q. Nguyen, A. Köhler, *J. Chem. Phys.* **2016**, *144*, 074904.
[45] D. Kroh, F. Eller, K. Schötz, S. Wedler, L. Perdigón-Toro, G. Freychet, Q. Wei, M. Dörr, D. Jones, Y. Zou, E. M. Herzig, D. Neher, A. Köhler, *Adv. Funct. Mater.* **2022**, *32*, 2205711.
[46] J. Liu, M. Arif, J. Zou, S. I. Khondaker, L. Zhai, *Macromolecules* **2009**, *42*, 9390.
[47] D. Raithel, S. Baderschneider, T. B. De Queiroz, R. Lohwasser, J. Köhler, M. Thelakkat, S. Kümmel, R. Hildner, *Macromolecules* **2016**, *49*, 9553.
[48] Z. Xu, K. S. Park, J. J. Kwok, O. Lin, B. B. Patel, P. Kafle, D. W. Davies, Q. Chen, Y. Diao, *Adv. Mater.* **2022**, *34*, 2203055.
[49] J. Lebert, E. M. Kratzer, A. Bourdick, M. Coric, S. Gekle, E. M. Herzig, *ACS Omega* **2018**, *3*, 6388.
[50] C. Enengl, S. Enengl, S. Pluczyk, M. Havlicek, M. Lapkowski, H. Neugebauer, E. Ehrenfreund, *ChemPhysChem* **2016**, *17*, 3836.
[51] Y. Furukawa, *J. Phys. Chem.* **1996**, *100*, 15644.
[52] J. Yamamoto, Y. Furukawa, *J. Phys. Chem. B* **2015**, *119*, 4788.
[53] Sigma-Aldrich, "Solvent Stabilizer Systems", https://www.sigmaaldrich.com/DE/de/technical-documents/technical-article/chemistry-and-synthesis/reaction-design-and-optimization/stabilizer-systems (accessed: December 2022).
[54] G. C. Vogel, R. S. Drago, *J. Chem. Educ.* **1996**, *73*, 701.
[55] S. Pröller, O. Filonik, F. Eller, S. Mansi, C. Zhu, E. Schaible, A. Hexemer, P. Müller-Buschbaum, E. M. Herzig, *ACS Appl. Mater. Interfaces* **2020**, *12*, 5219.
[56] P. O. Staneke, G. Groothuis, S. Ingemann, N. M. M. Nibbering, *Int. J. Mass Spectrom.* **1995**, *142*, 83.
[57] W. B. Knighton, E. P. Grimsrud, *J. Am. Chem. Soc.* **1992**, *114*, 2336.
[58] P. O. Staneke, G. Groothuis, S. Ingemann, N. M. M. Nibbering, *J. Phys. Org. Chem.* **1996**, *9*, 471.
[59] F. M. Keheze, D. Raithel, T. Wu, D. Schiefer, M. Sommer, R. Hildner, G. Reiter, *Macromolecules* **2017**, *50*, 6829.
[60] F. C. Spano, *Chem. Phys.* **2006**, *325*, 22.
[61] M. Gaus, Q. Cui, M. Elstner, *J. Chem. Theory Comput.* **2012**, *7*, 931.
[62] E. J. Baerends, SCM, ADF2022.01, SCM, Theoretical Chemistry, Vrije Universiteit, Amsterdam, The Netherlands **2012**, http://www.scm.com.
[63] G. Te Velde, F. M. Bickelhaupt, E. J. Baerends, C. Fonseca Guerra, S. J. A. Van Gisbergen, J. G. Snijders, T. Ziegler, *J. Comput. Chem.* **2001**, *22*, 931.
[64] A. D. Becke, *J. Chem. Phys.* **1993**, *98*, 5648.
[65] P. J. Stephens, F. J. Devlin, C. F. Chabalowski, M. J. Frisch, *J. Phys. Chem.* **1994**, *98*, 11623.
[66] T. H. Dunning, *J. Chem. Phys.* **1971**, *55*, 716.
[67] J. Gauss, J. F. Stanton, R. J. Bartlett, *J. Chem. Phys.* **1992**, *97*, 7825.